Simulation and validation of thermography inspection for components produced by additive manufacturing

Marta S. Carvalho[a,*], Ana P. Martins[a], Telmo G. Santos[a]

[a] *UNIDEMI, Departamento de Engenharia Mecânica e Industrial, NOVA School of Science and Technology, 2829-516 Caparica, Portugal*

Abstract

This work presents the validation of the numerical simulations performed to support the development of Non-Destructive Testing for parts produced by Additive Manufacturing. The most common defects of these components are the voids and delamination, for which the Active Transient Thermography is one of the most reliable Non-Destructive Testing methods. However, a systematic and scientific insight on the thermal phenomena involved on Active Transient Thermography is needed to optimize the Non-Destructive Testing inspection parameters. Several representative case studies were experimentally tested and numerically simulated. For the case studies, samples of the polymeric material Nylon PA-12 were produced by Fused Deposition Modelling. The commercial code ANSYS is used for the calculation with the Finite Element Method of the thermal transient problem, using a numerical model which includes the three primary modes of heat transfer: conduction, convection, and radiation. Numerical simulation allowed a deeper insight of the thermal phenomena involved in the Non-Destructive Testing inspection, and it proves to be a useful tool for the selection of Non-Destructive Testing parameters.

Keywords: Active thermography, Numerical simulation, Additive manufacturing, ANSYS, radiation

*Corresponding author
Email address: mip.carvalho@fct.unl.pt (Marta S. Carvalho)

1. Introduction

A considerable number of benefits related to additive manufacturing (AM) are motivating a rising research interest for these technologies. A major advantage of AM is the ability to produce customized components, with complex geometries without the general restrictions imposed by traditional manufacturing processes [1]. Despite its original application in rapid prototyping, for which materials with lower mechanical properties were used, 3D-printers can currently produce parts using several materials including metal [2, 3], ceramic [4] and composite materials [5, 6, 7] allowing the production of parts for demanding engineering solutions [8, 9].

Regardless of new developments on the materials for AM, polymers still one of the most widely used to produce 3D-printed components, with a noticeable research commitment to the characterization of parts manufactured by this technology [10]. Furthermore, the mechanical properties of the components have been improved through the local control of the deposition orientation and density [11], layer thickness and feed rate [12].

The greatest advantage of this technology, the complex shapes that may result from an AM production, represents at the same time a great challenge in the application of non-destructive testing (NDT) techniques [13]. Other challenges to NDT methods are the very low electrical and thermal conductivity of the polymeric materials. Despite some low conductivity, polymeric composite parts may be inspected without contact by eddy currents [14, 15], a faster and an image producer NDT technique should be target for such kind of inspections. The non-contact NDT technique that can overcome these limitations is the active thermography. Active Transient Thermography (ATT) is an NDT technique that uses an Infra-red (IR) camera that records spatial and temporal distribution of the temperature of the surface subject to a thermal gradient resulting from a transient or alternate change [16, 17]. The thermal energy can be transmitted by the direct contact between the specimen and a hot or cold object during a controlled time or by means of a blast of hot air or coolant. In this technique a flash tube or bulb is mostly used as the heat source. In the experimental set-up the heat source can be on the same side as the IR camera (reflection) or on the opposite side (transmission), as depicted in figure 1. The presence of defects changes the local thermal conductivity of the specimen and further disturbs the heat flow which allows the possibility of their detection. Therefore, in a transmission test, a defect such as a delamination will cause the temperature to rise more slowly on the monitored surface when compared to a non-defect zone. The defect detection is possible during the decreasing of the surface temperature where the region with defect has a decay rate lower than the rest of the specimen [16].

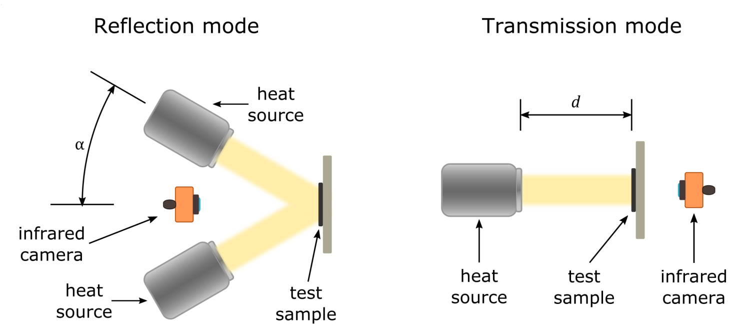

Figure 1: Schematic view of thermography inspection

NDT techniques usually require great effort and large number of experiments to achieve appropriate probe design and testing conditions. However, the cost efficiency of the NDT methods can be improved through appropriate numerical modelling. Aware of the advantages of using numerical models, several authors developed works using the finite element method to simulate the heat transfer phenomenon during thermography inspections. In those works, some commercial codes as MSC-Marc package [18], ANSYS [19], Abaqus [20], and COMSOL Multiphysics [21] were used. The numerical models were used to predict the detectability of defects [18], identify the more appropriate inspection parameters and optimise the evaluation process [22], estimate the defect size and shape [23], and foresee the frame that would best expose the defect [20].

However, in all the referred models, some simplifying assumptions were used, making the simulations quite different comparing to the real experimental inspection conditions: the effect of the heat source is simulated by applying a heat flux on the surface of the specimen that is exposed to the incidence of light coming from the heat source; the heat fluxes were either uniform in the cases of flat test specimens [18], or with a variable density, and the distribution values had to be experimentally obtained in the case of curved panels [19]. Therefore, these methodologies present a significant limitation, namely, they can only be used in the study of simple geometries and imply the existence of a great set of experimental testing whenever there are changes in the shape of the parts to be inspected.

In this work, a FEM model developed in ANSYS to solve the heat transient problem which covers the modelling of the radiating surfaces, including the heat source, as opposed to surface flux used by other authors [18, 19, 20, 21]. With the proposed model, the view factors are calculated during the routine, overcoming the difficulties regarding the complex geometry of the parts, which are inherent to the AM technology.

2. Experimental procedure

2.1. Sample description

As a result of the AM process, defects such as voids [24] and poor adhesion of the layers [25] may occur during the material deposition. To reproduce these common defects, the test specimen represented in figure 2 was selected to conduct simulations and the correspondent experimental testing for the validation of the numerical model. The specimen consists on a plate with a void created artificially, located at the centre of the test sample. The samples were produced by an *Ultimaker^3 Extended* Fused Deposition Modelling (FDM) 3D-printer using the polymeric material Nylon PA-12.

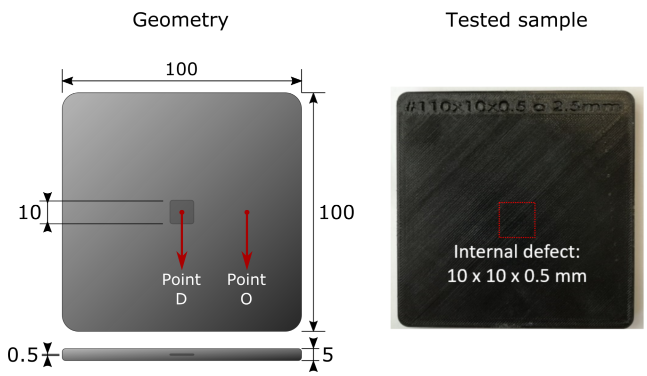

Figure 2: Test specimen for thermography evaluation

2.2. Experimental set-up

For the experimental procedure, two layouts were set for conducting both transmission and reflection modes of inspection. Layout A, shown in figure 3, has one heat source placed perpendicular to the test specimen at 160 mm, denoted by d in the scheme in figure 1. This layout was used for experiments in transmission mode, being the IR camera located on the rear side of the sample. Layout B, depicted in figure 3, has two heat sources positioned with a 35° angle, denoted by α in the scheme in figure 1. This layout is prepared to perform inspections in transmission and reflection modes, as the infrared camera can be placed on the same side of the heat sources (reflection), or on the opposite side (transmission).

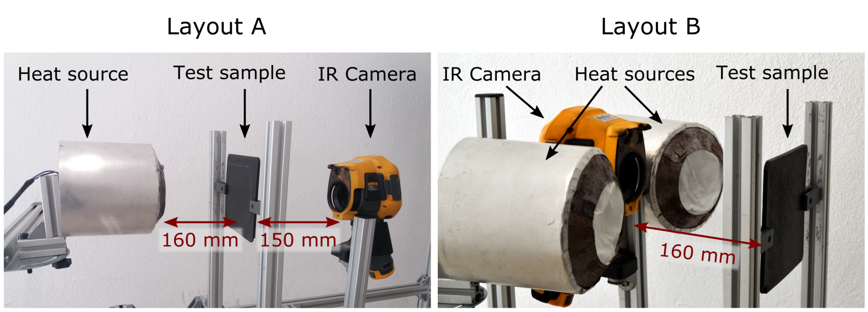

Figure 3: Experimental set-up

As heat sources, two Phillips IR300CH lamps of 300 W were used. The infrared camera Fluke Ti400 recorded the thermal response of the sample during the inspection, being the technical specifications listed in table 1. The camera works with a frame rate of 9 Hz, being this value appropriate to capture the transients in the measure specimen, since the maximum variation of temperature is 0.8° C/s.

Table 1: Technical specifications of the IR camera Fluke Ti400

Temperature measurement range	-20°C - 1200°C
Noise Equivalent Temperature Difference (NETD)	50 mK
Spectrum	7.5 – 14 μm
Accuracy	$\pm$ 2° C
Spatial resolution (iFOV)	2.62 mRad
iFOV on the object	196 μm/pixel

2.3. Testing procedures

In order to have representative values for the validation of the numerical model, three sets of experiments were conducted:

E1: Transmission test with 1 heat source (Layout A),

E2: Reflection test with 2 heat sources (Layout B),

E3: Transmission and reflection test with 2 heat sources (Layout B).

Since temperature can only be measured at one surface each time, E3 procedure was pre-pared to move the camera to the opposite side of the sample at successive tests to allow the shifting of the inspection mode (transmission and reflection). This procedure allows maintaining the test conditions (bulk temperature and initial temperature) as close as possible, so the identification of the parameters of the numerical model is done for both surfaces of the sample.

In all cases, the excitation time was 20 s, with the results being recorded for 150 s. These values were considered the most adequate, producing the best results, during the preliminary experimental tests performed for this purpose. Bulk temperature and initial temperature of the specimen were also registered at the beginning of every test. The following experiment would not begin before the stabilization of the temperature of the sample confirmed by a uniform measured temperature distribution on the surface of the sample, typically obtained after 15 minutes.

Both transmission and reflection modes demonstrated to be able to easily expose a defect with the stated characteristics, as depicted by figure 4, where the best contrast frame is presented for each evaluation mode. Nevertheless, higher temperature differences were found for reflection mode and the instant of the best contrast occurs earlier than for the transmission mode. From the inspection point of view, reflection mode is also preferable as access to the opposite surface might not always be possible for transmission mode to be used. The higher temperature difference for reflection mode was 1.2° C at 47 s; In the case of the transmission mode, the largest absolute contrast observed was 0.7° C at 53 s.

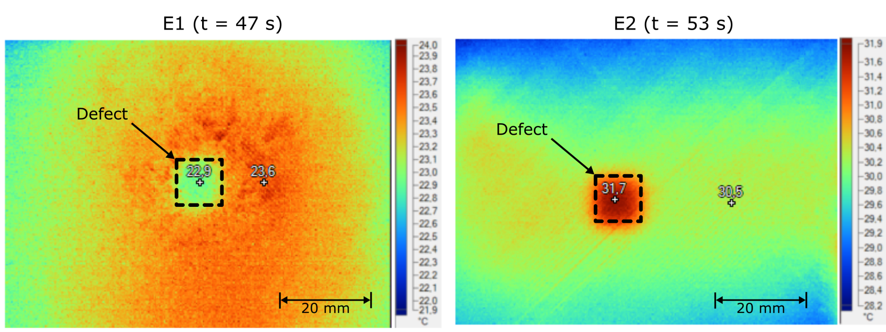

Figure 4: Frame of best temperature contrast achieved during experimental testing

3. Numerical model

For the simulation of the ATT NDT procedure, the commercial code ANSYS was used to calculate the finite element solution of the transient thermal problem [26] involving three primary modes of heat transfer: conduction, convection, and radiation. In ANSYS is possible to perform a heat transient analysis including the radiation using several methods [27]. One of these methods uses the radiation link element Link 31 for the calculation of the radiant heat transfer between two points [28]. This method was used in the work of [29] for simulating the temperature field in the main reflector of a radio telescope considering multiple environmental parameters and self-shadows. For the radiation link element, the effective radiating surface area and the view factor should be specified by the user. An alternative method is using surface effect elements, for which the view factor can be either calculated from the position of the elements or given as an input, being limited to radiation transfer between an element and a point [28]. Our goal nonetheless is to have the form factors calculated by the code for to arbitrary surfaces radiating to each other, therefore the radiation matrix method is selected, which uses elements (Link 33) overlaying the boundaries of the mesh in the radiating surfaces of the 2D model as illustrated in figure 5.

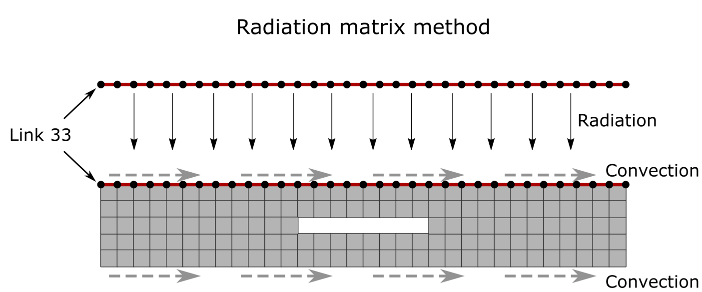

Figure 5: Schematic representation of overlaying elements in the radiating surfaces for the radiation matrix method (not in scale)

To model the heat transferred from the heat source to the test specimen, the approach used here considers the heat transfer rate Q [W] between surfaces i and j, radiating to each other as determined by equation 1,

$$Q_i = \frac{1}{\frac{1-\epsilon_i}{A_i \epsilon_i} + \frac{1}{A_j F_{ij}} + \frac{1-\epsilon_j}{A_j \epsilon_j}} \sigma (T_i^4 - T_j^4) \tag{1}$$

where A [m^2] is the area of the surface, ϵ [-] is the effective emissivity and σ [$W/m^2 \cdot K^4$] is the Stefan–Boltzmann constant. The view factor, F_{ij} [-], is defined as the fraction of total radiant energy that leaves surface i which arrives directly on surface j can be expressed by equation 2,

$$F_{ij} = \frac{1}{A_i} \int_{A_i} \int_{A_j} \frac{\cos\theta_i \cos\theta_j}{\pi r^2} dA_j dA_i \tag{2}$$

where r [m] is the distance between the differential surfaces, N is the surface normal and θ [rad] is the angle between N and r. The sample was meshed using 8 node plane elements with a regular size of 0.25 mm. This value results in a mapped mesh of 400×40 elements and was obtained after performing mesh convergence tests. The selected mesh was considered sufficiently accurate when the numerical solution provided by the model presents negligible changes as the mesh refinement increases. Regarding time discretization, a time step of 0.1 s was used to compute the analysis solution.

The prescribed boundary conditions are the nodal temperatures of the heat source and the convection applied to all the surfaces of the modelled specimen. Since experimental procedures for transmission and reflection modes were executed separately, the film coefficient (h), the bulk temperature (T_B) and initial temperature of the test specimen (T_p) had to be tuned to the values listed in table 2 to be consistent to the corresponding environment conditions.

Table 2: Prescribed boundary conditions

Procedure	Film coefficient (h) $W/m^2 \cdot °C$	Bulk temp. (T_B) °C	Initial temp. (T_p) °C
E1	12.5	20.9	21.4
E2	13.0	23.9	24.4
E3	10.5	24.5	24.4

The modelled sample and heat sources are assumed as grey diffuse bodies with emissivity of 0.95. The specimen model is considered to have plane element behaviour and isotropic material properties that do not vary for the analysis temperature range. The material properties for PA-12 of interest for the purposes of heat transfer simulation are presented in table 3.

Table 3: PA-12 material properties for the temperature range of the NDT procedures

Conductivity (K)	Density (ρ)	Specific heat (C_p)
0.22 $W/m^2 \cdot K$	1100 kg/m^3	1590 $J/kg \cdot K$

4. Results and Discussion

The validation of the numerical model was performed by comparing the temperature measurements during the experimental procedure E3 with the values obtained in the simulation. The correlation between results was implemented in two points depicted in figure 2 – one point above the defect (point D) and another at half distance between the edge of the defect and the end of the sample (point O). This positioning corresponds to a distance between points of 27.5 mm.

In figure 6 are depicted the time history of the temperature measured for reflection and transmission modes. To observe thereafter the shadowed regions correspond to the representation of the results of several experiments, and the solid line corresponds to the average of the measurements. Both simulation results show a good correlation with the experimental data. For the reflection mode simulation, the peak temperature is 31.98° C and occurs at 20 s, correspondent to the final period of excitation. Furthermore, the relative deviation of the simulation results is below 4.8% for reflection and transmission modes.

In the point of view of the thermography inspection process, the detection of the defects is visible due to the contrast presented. Mathematically this is achieved with difference of the temperature between point D and point O, being plotted in figure 7 for reflection and transmission modes. Again, both simulation results show a good correlation with the experimental data, being the relative

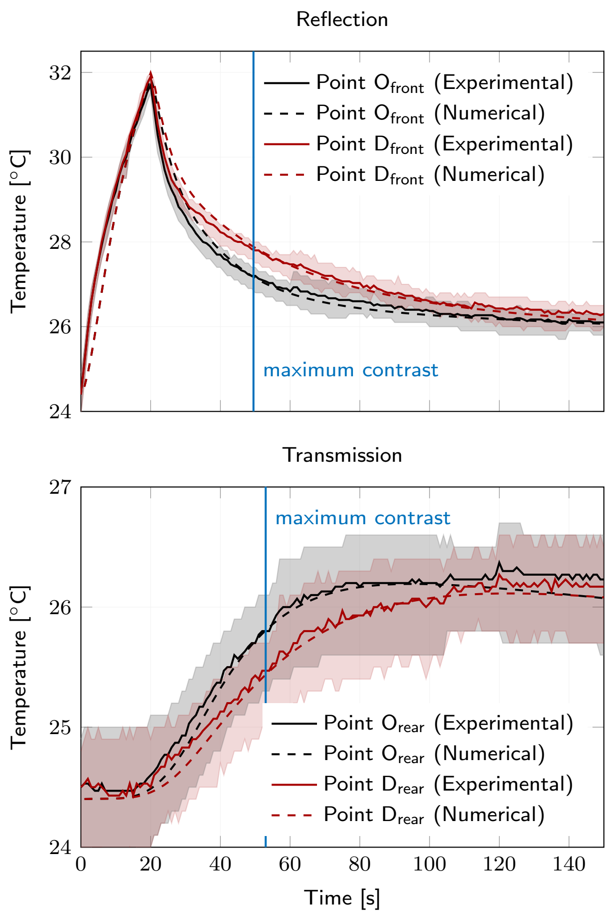

Figure 6: Temperature vs Time during experimental procedure E3 and numerical simulation

deviation at the maximum temperature difference below 8.6%. Consequently, the numerical model correspondent to experimental procedure E3 is validated.

With a validation completed for E3 procedure, a suitability of the model for different inspection conditions was verified, comparing the thermal contrast for the E2 and E1 procedures. The temperature differences for reflection and transmission modes are plotted in figure 8. Once more, a good correlation of the simulation results with the experimental data was achieved, being the relative deviation at the maximum temperature difference below 7.9%.

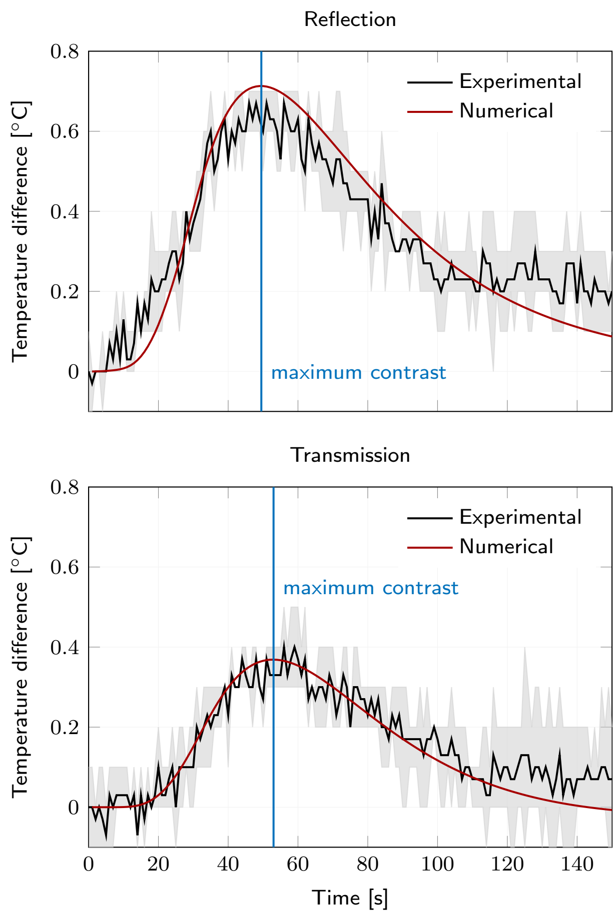

Figure 7: Temperature difference vs Time during experimental procedure E3 and numerical simulations

An additional output is an insight of the temperature distribution of the test sample and the temperature profile for the surface inspected for each time instant. For the time instant of maximum contrast for rear surface (50 s), which is presented in figure 9 for E1 procedure and simulation results with the presented model (straight line) and with a simplified model (dash line), is possible to detect not only the location of the defect but also the length of it, due to the clear temperature variation in its region. For the same instant, the temperature scattering inside the specimen is illustrated in figure 10.

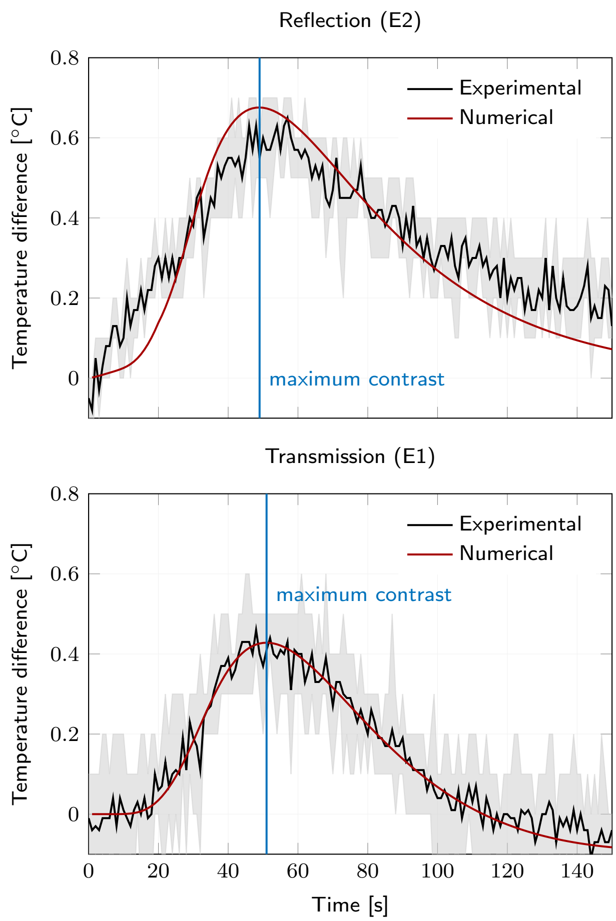

Figure 8: Temperature difference vs Time during experimental procedures E2 and E1 and numerical simulations

The simplified model used a uniform heat flux, corroborating the better curve fitted along the surface presented with the proposed model that includes the radiation. Moreover, the specimen used here has a flat geometry, but the heat source in experimental procedure E1 is very close leading to a non-uniform heat flux, concentrated in the incidence area. This heat flux distribution is better described when the radiation matrix method is used for the calculation of the view factors between the surfaces. When the simulation of the inspec-

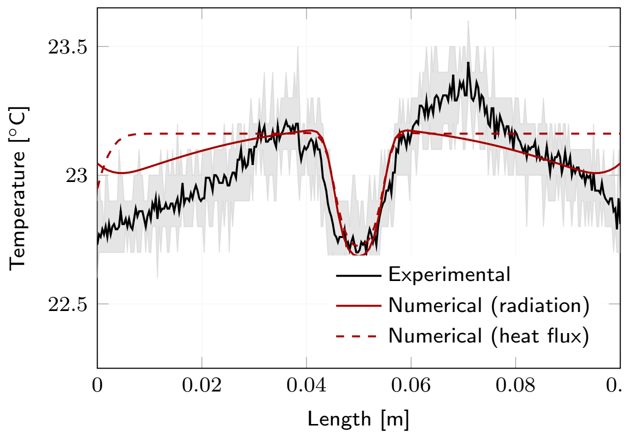

Figure 9: Temperature profile of rear surface of the specimen after 50 s of experimental procedure E1 and numerical simulation

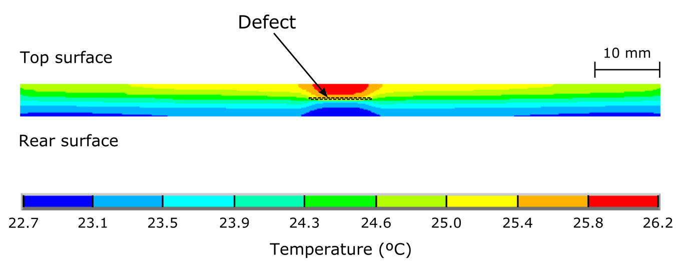

Figure 10: Simulated temperature distribution inside the test specimen after 50 s

tion of more complex geometries is required, for which the incident heat flux along the surface is hard to perceive beforehand, the importance of using this method increases substantially. A comparison between the simulation for the NDT inspection of a curved plate with the proposed model versus the simplified model with a uniform heat flux is made. For the simulations, one heat source is positioned at the distance used in Layout A. In table 4 are represented the temperature distributions after 20 s (end of excitation time) and for the time instant correspondent to maximum contrast (50 s) for radiation and heat flux models. For the end of excitation time, since the heat flux is not uniform along the surface and the temperature is superior at the centre (closer to the heat source), the displayed results reveal that the proposed model is more realistic. Although a non-uniform heat flux may be applied, the dependency of experimental data when changes are made to geometry of the testing component make this method unsuitable for the development of tools to support the selection of the appropriate inspection parameters for generalized AM products. For the time instant correspondent to maximum contrast (50 s), the temperature distributions for both models evince the differences of the thermal response. It can be observed that notwithstanding the bigger temperature increase in the radiation model, a clearer contrast is obtained in the simplified model which could result in misleading conclusion on the detectability of the defect.

Table 4: Simulated temperature distribution for a curved test specimen

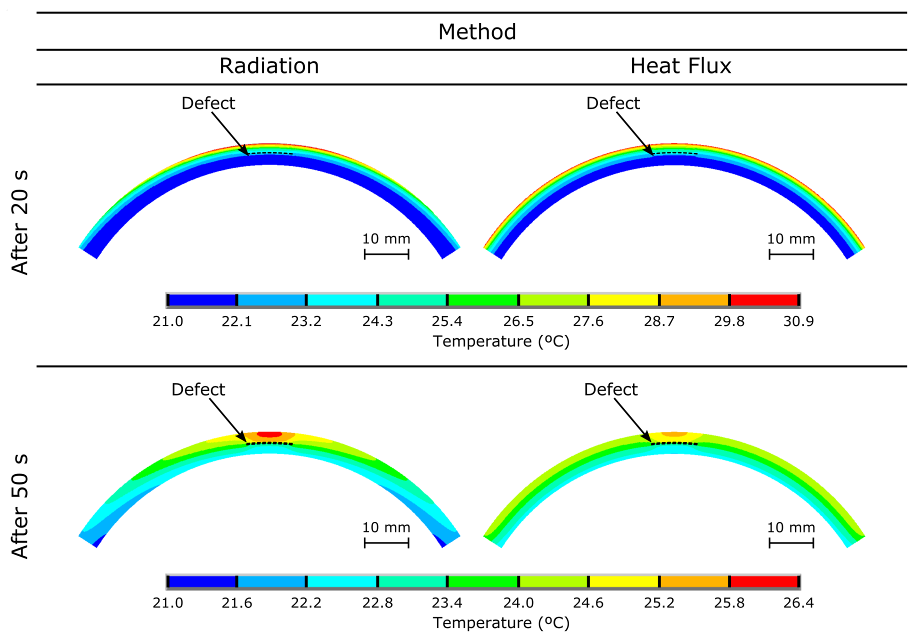

5. Conclusions

In this work is presented a finite element model that considers the three primary modes of heat transfer to simulate the transient of an active thermography Non-Destructive Testing inspection method for polymer parts produced by Additive Manufacturing technology. The numerical model presented relative deviations below 8.6% for different experimental inspection procedures conducted here, being thereby validated. Furthermore, the presented model includes the radiation phenomenon, being the great importance of the proposed model examined with the simulation of the inspection of complex geometries that are common to obtain with Additive Manufacturing technology. Comparison between simulation results of the proposed model and a simplified model using a uniform heat flux emphasize the importance of including the radiation to obtain more realistic thermal responses from the testing samples. The proposed numerical model is the backbone of the methodology to simulate the transient heat transfer of parts with complex geometry in order to be applied in the development of improved inspection tools.

Acknowledgements

Authors gratefully acknowledge the funding of Project POCI-01-0145-FEDER-016414 (FIBR3D), cofinanced by Programa Operacional Competitividade e Internacionalização and Programa Operacional Regional de Lisboa, through Fundo Europeu de Desenvolvimento Regional (FEDER) and by National Funds through Fundação para a Ciência e a Tecnologia (FCT - MCTES). MSC and TGS acknowledge FCT - MCTES for its financial support via the project UID/EMS/00667/2019 (UNIDEMI).

References

References

[1] J. Holmström, J. Partanen, J. Tuomi, M. Walter, Rapid manufacturing in the spare parts supply chain: alternative approaches to capacity deployment, Journal of Manufacturing Technology Management 21 (6) (2010) 687–697. doi:https://doi.org/10.1108/17410381011063996.

[2] W. E. Frazier, Metal additive manufacturing: a review, Journal of Materials Engineering and Performance 23 (6) (2014) 1917–1928. doi:https://doi.org/10.1007/s11665-014-0958-z.

[3] A. Lopez, R. Bacelar, I. Pires, T. G. Santos, J. P. Sousa, L. Quintino, Non-destructive testing application of radiography and ultrasound for wire and arc additive manufacturing, Additive Manufacturing 21 (2018) 298–306. doi:https://doi.org/10.1016/j.addma.2018.03.020.

[4] J. Deckers, J. Vleugels, J.-P. Kruth, Additive manufacturing of ceramics: a review, Journal of Ceramic Science and Technology 5 (4) (2014) 245–260. doi:10.4416/JCST2014-00032.

[5] F. Ning, W. Cong, J. Qiu, J. Wei, S. Wang, Additive manufacturing of carbon fiber reinforced thermoplastic composites using fused deposition modeling, Composites Part B: Engineering 80 (2015) 369–378. doi:https://doi.org/10.1016/j.compositesb.2015.06.013.

[6] X. Wang, M. Jiang, Z. Zhou, J. Gou, D. Hui, 3d printing of polymer matrix composites: A review and prospective, Composites Part B: Engineering 110 (2017) 442–458. doi:https://doi.org/10.1016/j.compositesb.2016.11.034.

[7] L. Blok, M. Longana, H. Yu, B. Woods, An investigation into 3d printing of fibre reinforced thermoplastic composites, Additive Manufacturing 22 (2018) 176–186. doi:https://doi.org/10.1016/j.addma.2018.04.039.

[8] J.-Y. Lee, J. An, C. K. Chua, Fundamentals and applications of 3d printing for novel materials, Applied Materials Today 7 (2017) 120–133. doi:https://doi.org/10.1016/j.apmt.2017.02.004.

[9] S. Singh, S. Ramakrishna, R. Singh, Material issues in additive manufacturing: A review, Journal of Manufacturing Processes 25 (2017) 185–200. doi:https://doi.org/10.1016/j.jmapro.2016.11.006.

[10] J. R. C. Dizon, A. H. Espera, Q. Chen, R. C. Advincula, Mechanical characterization of 3D-printed polymers, Additive Manufacturing 20 (2018) 44–67. doi:https://doi.org/10.1016/j.addma.2017.12.002.

[11] L. Li, Q. Sun, C. Bellehumeur, P. Gu, Composite modeling and analysis for fabrication of FDM prototypes with locally controlled properties, Journal of manufacturing processes 4 (2) (2002) 129–141. doi:https://doi.org/10.1016/S1526-6125(02)70139-4.

[12] J. Chacón, M. Caminero, E. García-Plaza, P. Núñez, Additive manufacturing of pla structures using fused deposition modelling: Effect of process parameters on mechanical properties and their optimal selection, Materials & Design 124 (2017) 143–157. doi:https://doi.org/10.1016/j.matdes.2017.03.065.

[13] Z. Quan, A. Wu, M. Keefe, X. Qin, J. Yu, J. Suhr, J.-H. Byun, B.-S. Kim, T.-W. Chou, Additive manufacturing of multi-directional preforms for composites: opportunities and challenges, Materials Today 18 (9) (2015) 503–512. doi:https://doi.org/10.1016/j.mattod.2015.05.001.

[14] M. A. Machado, K.-N. Antin, L. S. Rosado, P. Vilaça, T. G. Santos, Contactless high-speed eddy current inspection of unidirectional carbon fiber reinforced polymer, Composites Part B: Engineering 168 (2019) 226–235. doi:https://doi.org/10.1016/j.compositesb.2018.12.021.

[15] K.-N. Antin, M. A. Machado, T. G. Santos, P. Vilaça, Evaluation of different non-destructive testing methods to detect imperfections in unidirectional carbon fiber composite ropes, Journal of Nondestructive Evaluation 38 (1) (2019) 23. doi:https://doi.org/10.1007/s10921-019-0564-y.

[16] M. R. Jolly, A. Prabhakar, B. Sturzu, K. Hollstein, R. Singh, S. Thomas, P. Foote, A. Shaw, Review of non-destructive testing (ndt) techniques and their applicability to thick walled composites, Procedia CIRP 38 (2015) 129–136. doi:https://doi.org/10.1016/j.procir.2015.07.043.

[17] Q. Tang, J. Dai, C. Bu, L. Qi, D. Li, Experimental study on debonding defects detection in thermal barrier coating structure using infrared lock-in thermographic technique, Applied Thermal Engineering 107 (2016) 463–468. doi:https://doi.org/10.1016/j.applthermaleng.2016.07.008.

[18] F. Mabrouki, M. Genest, G. Shi, A. Fahr, Numerical modeling for thermographic inspection of fiber metal laminates, NDT & E International 42 (7) (2009) 581–588. doi:https://doi.org/10.1016/j.ndteint.2009.02.010.

[19] P. D. Pastuszak, Characterization of defects in curved composite structures using active infrared thermography, Procedia Engineering 157 (2016) 325–332. doi:https://doi.org/10.1016/j.proeng.2016.08.373.

[20] K. Ghadermazi, M. Khozeimeh, F. Taheri-Behrooz, M. Safizadeh, Delamination detection in glass–epoxy composites using step-phase thermography (spt), Infrared Physics & Technology 72 (2015) 204–209. doi:https://doi.org/10.1016/j.infrared.2015.08.006.

[21] M. Grosso, J. E. Lopez, V. M. Silva, S. D. Soares, J. M. Rebello, G. R. Pereira, Pulsed thermography inspection of adhesive composite joints: computational simulation model and experimental validation, Composites Part B: Engineering 106 (2016) 1–9. doi:https://doi.org/10.1016/j.compositesb.2016.09.011.

[22] J. Peeters, C. Ibarra-Castanedo, F. Khodayar, Y. Mokhtari, S. Sfarra, H. Zhang, X. Maldague, J. J. Dirckx, G. Steenackers, Optimised dynamic line scan thermographic detection of cfrp inserts using fe updating and pod analysis, NDT & E International 93 (2018) 141–149. doi:https://doi.org/10.1016/j.ndteint.2017.10.006.

[23] J. Peeters, C. Ibarra-Castanedo, S. Sfarra, X. Maldague, J. Dirckx, G. Steenackers, Robust quantitative depth estimation on cfrp samples using active thermography inspection and numerical simulation updating, NDT

& E International 87 (2017) 119–123. doi:https://doi.org/10.1016/j.ndteint.2017.02.003.

[24] S. Guessasma, W. Zhang, J. Zhu, S. Belhabib, H. Nouri, Challenges of additive manufacturing technologies from an optimisation perspective, International Journal for Simulation and Multidisciplinary Design Optimization 6 (2015) A9. doi:https://doi.org/10.1051/smdo/2016001.

[25] O. Es-Said, J. Foyos, R. Noorani, M. Mendelson, R. Marloth, B. Pregger, Effect of layer orientation on mechanical properties of rapid prototyped samples, Materials and Manufacturing Processes 15 (1) (2000) 107–122. doi:https://doi.org/10.1080/10426910008912976.

[26] J. N. Reddy, D. K. Gartling, The finite element method in heat transfer and fluid dynamics, CRC press, 2010. doi:https://doi.org/10.1201/9781439882573.

[27] P. Kohnke, Ansys mechanical apdl theory reference, release 16.0, Inc., Canonsburg, PA, USA(2015) (2015).

[28] P. Kohnke, Ansys thermal analysis guide, release 16.0, Inc., Canonsburg, PA, USA(2015) (2015).

[29] D. Chen, H. Qian, H. Wang, G. Zhang, F. Fan, S. Shen, Non-uniform temperature field measurement and simulation of a radio telescope's main reflector under solar radiation, Applied Thermal Engineering 111 (2017) 1330–1341. doi:https://doi.org/10.1016/j.applthermaleng.2016.10.032.